ELSEVIER

Journal of Organometallic Chemistry 549 (1997) 55–72

Journal of Organometallic Chemistry

Optically active pentanuclear wing-tip butterfly heterotrimetallic clusters[1]

S.P. Gubin [a,*], T.V. Galuzina [a], I.F. Golovaneva [a], A.P. Klyagina [a], L.A. Polyakova [a], O.A. Belyakova [b], Ya.V. Zubavichus [b], Yu.L. Slovokhotov [b]

[a] *Institute of General and Inorganic Chemistry, Russian Academy of Sciences, 117907 Moscow, Russian Federation*
[b] *Institute of Organoelement Compounds, Russian Academy of Sciences, 117813 Moscow, Russian Federation*

Received 28 February 1997

Abstract

The pentanuclear heterotrimetallic clusters of formula $Fe_3MC(CO)_{12}M'L$ {M = Co, M' = Au, L = PPh_3 (**XIV**); M = Co, M' = Pd, L = η^3-C_3H_5 (**XV**); M = Co, M' = Pd, L = η^3-β-pinenyl, $C_{10}H_{15}$ (**I**); M = Rh, M' = Au, L = PPh_3 (**XVI**); M = Rh, M' = Pd, L = η^3-C_3H_5 (**XVII**); M = Rh, M' = Pd, L = η^3-$C_{10}H_{15}$ (**II**)} have been obtained by the addition of corresponding M'L fragments to heterometallic butterfly $[Fe_3MC(CO)_{12}]^-$, where M = Co (**XI**) or Rh (**X**); the butterfly **XI** has been isolated in reductive degradation of Co-containing clusters $[Fe_3Co_3C(CO)_{15}]^-$ or $[Fe_4CoC(CO)_{14}]^-$. The X-ray crystal structures of **XIV** and **XV** have been determined. Both structures have approximately the same pentanuclear heterotrimetallic cluster cores with M'L groups in bridging position linking wing tips. According to the refinement data, the Co atoms in **XIV** and **XV** are placed in the basal position of the butterfly. EXAFS data for **XV** suggest a structural flexibility of the metal core in solution. Absorption (AB) and circular dichroism (CD) spectra of two optically active clusters **I** and **II** with the same 'wing-tip' butterfly structure were investigated and compared with those for the starting $[Pd(\eta^3$-β-$C_{10}H_{15})Cl]_2$ chiral complex. The noticeable Cotton effects (CE) in the CD spectra induced in electron transitions of cluster metallochromophores demonstrate a strong manifestation of the vicinal optical activity. © 1997 Elsevier Science S.A.

Keywords: Pentanuclear heterotrimetallic clusters; 'Wing-tip' butterfly structure; Optically active clusters; X-ray crystal structure; Iron; Cobalt; Palladium; Rhodium; Gold

1. Introduction

Heteropolymetallic clusters with a nuclearity of 4 to 6 are good model compounds in the study of structures, stereochemistry and optical activity of polynuclear complexes. Recently, the most impressive progress was achieved in the field of synthesis of carbonyl clusters with an interstitial C atom, in which a variety of synthetic routes to clusters with a desirable molecular geometry (including chiral species) was developed. Typical methods of synthesis of carbide clusters include the metal atom substitution, the controlled degradation of metal polyhedra and the following addition of heterometallic vertices. To date, this scheme allowed to obtain and characterize more than 60 various heterometallic carbide carbonyl clusters containing up to four different metal atoms in a cluster core [1].

A replacement of one metal vertex in a polyhedron by the atom of another metal (close or distant in the Periodic Table) gives an opportunity to check the existing models of optical activity and to look for correlation of optical properties with the electronic structure of the cluster. A series of electron transitions in the visible region makes a metal cluster core as a convenient chromopore. Insertion of a metal atom already coordinated with a chiral ligand into a cluster polyhedron therefore allows to study an interaction between the cluster and ligand chromopores. Preliminary data

* Corresponding author.

[1] This paper is dedicated to the memory of Prof. Yuri T. Struchkov as a tribute to his great contribution to structural chemistry. One of the authors (S.P.G.) was related to Yuri Struchkov with many years of friendship and a fruitful cooperation. Prof. Struchkov was a highly esteemed teacher to Yu.L.S.; he also encouraged the students Ya.V.Z. and O.A.B. in their first steps in structural studies. For all of us he was an outstanding scholar, whose faithful attitude towards science, profound knowledge and industrious work always earned our admiration.

PII S0022-328X(97)00490-7

showed that the mixing of metal and ligand transitions may promote optical activity even for achiral metal cores within an asymmetric ligand environment [2].

The above considerations determine a growing interest in chiroptical properties and spectra of metal clusters. However, only few clusters with chiral metal framework and/or ligand environment were studied up to now, and the data available for their atomic and electronic structures, as well as spectra, are still insufficient for serious theoretical analysis [3]. Further studies in this field are therefore required.

This paper gives a brief review of our recent results concerning synthesis and stereochemistry of heterometallic clusters of the wing-tip butterfly type. The geometry of metal core in these compounds facilitates both asymmetry and flexibility of their molecules, creating the possibility for unusual properties of some clusters in this class. Studies of circular dichroism (CD) spectra of chiral butterflies may be especially informative, since a low symmetry of metal polyhedron provides a well-developed band structure. Stepwise vertex substitution in the metal core probably gives the most promising way of the synthesis of heterometallic carbide clusters [4]. This process is usually believed to occur when the metal vertex M is removed from the n-atomic core M_n with the following addition of another metal vertex M′ to the $(n-1)$-nuclear cluster formed in all cases with the retention of initial geometry of metal core (Scheme 1, path A). We have found, however, that the stepwise addition of metal atoms to the closest environment of the interstitial atom may proceed in a more complicated way. For some metals a consecutive degradation of the initial M_n cluster core and an addition of another M′ atom to M_{n-1} moiety therefore gives n-nuclear clusters $M'M_{n-1}$ of a different geometry. A typical example of such transformations is the synthesis of heteronuclear wing-tip butterfly clusters from a heteronuclear butterfly species (Scheme 1, path B).

Systematic investigations of this new reaction pathway allowed us to characterize a series of the novel wing-tip butterfly clusters, including the first chiral members of this family $Fe_3MPdC(CO)_{12}(\eta^3\text{-}C_{10}H_{15})$ [where M = Co (**I**) and Rh (**II**)]. Structures of the compounds in the solid state and in a solution were determined from single crystal X-ray, EXAFS and CD data, as well as from electrochemistry data and ESR spectra. Chiroptical properties of the binuclear complex [(β-pinenyl)PdCl]$_2$ (**III**), which enters into the wing-bridging organometallic units of **I** and **II**, were also reinvestigated by us. Several preliminary results of these studies were published elsewhere [2,5,6].

2. Experimental

All manipulations in the preparation and purification of clusters were carried out under argon using standard procedures. $[Fe_6C(CO)_{16}]^{2-}$, $[Rh(CO)_2Cl]_2$ (**IV**), $[RhCl(CO)(PPh_3)_2]$ (**V**), $(Me_4N)[Fe_4CoC(CO)_{14}]$ (**VI**), $AuPPh_3Cl$ (**VII**), $[Pd(C_3H_5)Cl]_2$ (**VIII**), $[Pd(\beta\text{-}C_{10}H_{15})Cl]_2$ (**III**), $(PPN)_2[Fe_3(CO)_9CCO]$ (**IX**), and $(PPN)[Fe_3RhC(CO)_{12}]$ (**X**) were obtained by the known methods [7–16]. Tetrahydrofuran (THF) and diglyme were purified by distillation with sodium benzophenone ketyl. All other solvents were of grades 'chemically pure' or 'spectroscopically pure.' PPh_3 was recrystallized from hot ethanol.

2.1. Preparation of $(Me_4N)[Fe_3CoC(CO)_{12}]$ (XI)

$(Me_4N)[Fe_4CoC(CO)_{14}]$ (**VI**) (0.1 g, 0.13 mmol) was added to a saturated solution of EtOH/KOH (50 ml). After 5 min of stirring (at room temperature), the color of the solution changed from brown to red. The mixture was filtered into a saturated solution of Me_4NBr/H_2O. The precipitate was filtered off and dissolved in CH_2Cl_2. The solvent was removed in vacuo, the residue was washed with hexane and the product was recrystallized from CH_2Cl_2 at −5°C. Yield 20% (0.02 g). Anal. Found: Fe, 25.80; Co, 9.05; C, 32.00. Calcd. for $C_{17}H_{12}CoFe_3NO_{12}$: Fe, 25.89; Co, 9.09; C, 31.45%.

2.2. Preparation of $Fe_3CoRhC(CO)_{14}$ (XII)

Equimolar quantities (~ 0.05 mmol) of $(Me_4N)[Fe_3CoC(CO)_{12}]$ (**XI**) and $[Rh(CO)_2Cl]_2$ (**IV**) were dissolved in CH_2Cl_2. The mixture was stirred for 5 min at room temperature, the color of the solution

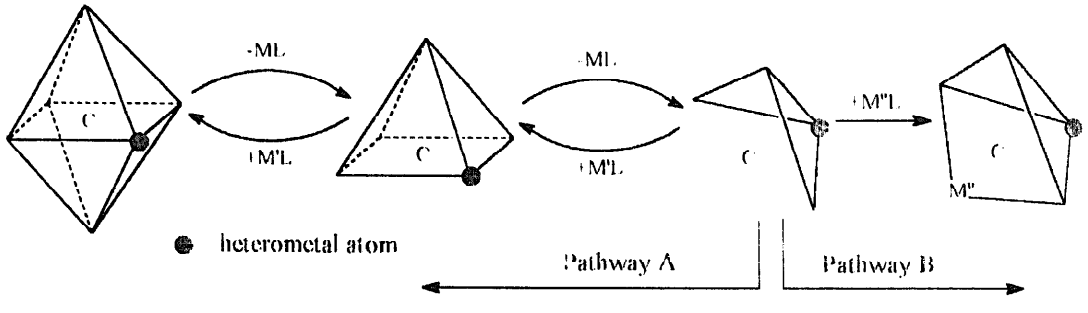

Scheme 1.

changed from red to brown. After crystallization from hexane, the cluster $Fe_3CoRhC(CO)_{14}$ **(XII)** was obtained. Yield 80%. Anal. Found: Fe, 22.90; Co, 8.09; Rh, 13.49; C, 25.03. Calcd. for $C_{15}CoFe_3O_{14}Rh$: Fe, 22.88; Co, 8.04; Rh, 13.03; C, 25.52%.

2.3. Substitution of CO by PPh_3 in $Fe_3CoRhC(CO)_{14}$

The two-fold excess of PPh_3 was added to a pentane solution of $Fe_3CoRhC(CO)_{14}$ **(XII)** (0.1 g, 0.14 mmol). The mixture was stirred for 5 min at room temperature, the color of the solution (brown) did not change, but in this case the white precipitate was formed. The solution was decanted and concentrated in vacuo, and the black crystals were filtered off. The product **(XIII)** obtained was recrystallized from hexane at room temperature. Yield 50% (0.07 g). [2]

2.4. Preparation of $Fe_3CoRhC(CO)_{13}$ PPh_3 (XIII)

The 1.5-fold excess of $[RhCl(CO)(PPh_3)_2]$ **(V)** was added to $(Me_4N)[Fe_3CoC(CO)_{12}]$ **(XI)** in CH_2Cl_2. The mixture was stirred for 120 h at room temperature, the color of the solution changed from red to brown. The solution was concentrated in vacuo, the black crystals were filtered off. Yield 50% (0.07 g). MS m/z 967.8 (M^+), calcd. 967.8 amu.

2.5. Preparation of $Fe_3CoAuC(CO)_{12}PPh_3$ (XIV)

The 1.5-fold excess of $AuPPh_3Cl$ **(VII)** was added to $(Me_4N)[Fe_3CoC(CO)_{12}]$ **(XI)** (0.1 g, 0.15 mmol) dissolved in CH_2Cl_2 (10 ml) at 25°C. The suspension was stirred at room temperature for 5 min until the initially deep red solution turned brown. The solvent was removed and the residual solid was extracted with pentane. Filtration followed by evaporation of the solution to dryness yielded $Fe_3CoAuC(CO)_{12}PPh_3$ (0.12 g, 0.12 mmol, 80%). After recrystallization from pentane (−5°C), a black crystalline compound was obtained. Anal. Found: C, 36.43; H, 1.42. Calcd. for $Fe_3AuCoC_{31}H_{15}PO_{12}$: C, 36.01; H, 1.46%.

2.6. Preparation of $Fe_3CoPdC(CO)_{12}$ (η^3-C_3H_5) (XV)

$(Me_4N)[Fe_3CoC(CO)_{12}]$ **(XI)** (0.1 g, 0.15 mmol) was dissolved in CH_2Cl_2 (10 ml) at 25°C. The 1.5-fold excess of $[Pd(C_3H_5)Cl]_2$ **(VIII)** was added and the suspension was stirred at room temperature for 5 min until the initially deep red solution turned brown. The solvent was removed and the residual solid was extracted with pentane. Filtration followed by evaporation of the solution to dryness yielded $Fe_3CoPdC(CO)_{12}(C_3H_5)$ (0.09 g, 0.12 mmol, 80%). After recrystallization from pentane (−5°C), a black crystalline compound was obtained. Anal. Found: C, 26.91; H, 0.65. Calcd. for $Fe_3CoPdC_{16}H_5O_{12}$: C, 26.59; H, 0.69%.

2.7. Preparation of $Fe_3CoPdC(CO)_{12}$ (η^3-$C_{10}H_{15}$) (I)

Cluster **I** was prepared in a way similar to **XV**. The 1.5-fold excess of $[Pd(\eta^3\text{-}C_{10}H_{15})Cl]_2$ **(III)** was added to **XI** in CH_2Cl_2. Yield 80% (0.1 g). MS $m/z = 816$ (M^+), calcd. 816 amu.

2.8. Preparation of $Fe_3RhAuC(CO)_{12}$ PPh_3 (XVI)

$(PPN)[Fe_3RhC(CO)_{12}]$ **(X)** (0.1 g, 0.09 mmol) was dissolved in CH_2Cl_2 (5 ml) at 25°C. The 1.2-fold excess of $AuPPh_3NO_3$ was added and the suspension was stirred at room temperature for 5 min. The solvent was removed in vacuo, the residue was eluated with CH_2Cl_2/hexane mixture (1:3) from a silica gel column. Yield: 52% (0.047 g). Anal. Found: C, 35.00; H, 1.72; Fe, 15.85. Calcd. for $Fe_3RhAuC_{31}H_{15}PO_{12}$: C, 34.55; H, 1.40; Fe, 15.54%.

2.9. Preparation of $Fe_3RhPdC(CO)_{12}$ (η^3-C_3H_5) (XVII)

XVII was synthesized in a way similar to **XVI** from $(PPN)[Fe_3RhC(CO)_{12}]$ **(X)** (0.1 g) and equimolar amount of $[Pd(C_3H_5)Cl]_2$ **(VII)** (0.03 g). Yield: 50% (0.03 g). Anal. Found: C 25.40; H 1.00; Fe 21.40. Calcd. for $Fe_3RhPdC_{16}H_5O_{12}$: C, 25.07; H, 0.65; Fe, 21.87%. MS FAB $m/z = 766$ (M^+), calcd. 766.029 amu.

2.10. Preparation of $Fe_3RhPdC(CO)_{12}$ (η^3-$C_{10}H_{15}$) (II)

Cluster **II** was synthesized in a way similar to **XVI** from $(PPN)[Fe_3RhC(CO)_{12}]$ **(X)** (0.1 g) and equimolar amount of **III** (0.05 g). Yield 60% (0.05 g). Anal. Found: C, 32.50; H, 2.00; Fe, 19.00. Calcd. for $Fe_3RhPdC_{23}H_{15}O_{12}$: C, 32.10; H, 1.74; Fe, 19.48%

2.11. Spectroscopy

IR spectra were recorded on a spectrometer Specord 75IR (in Nujol mulls or CH_2Cl_2 and hexane solutions) in the range 400–4000 cm^{-1}. The C–O and M–C vibrational frequencies for all clusters synthesized are shown in the Table 1.

The electrochemical generation of anion radicals and the monitoring of their ESR spectra were performed in

[2] The dark crystalline main product always contains an unremovable admixture of PPh_3 as a white powder. For mass-spectrometry and X-ray studies, dark crystals of **XIII** were picked manually from the bulk of the product.

e

Table 1
IR spectra of clusters studied in the region of ν_{CO} and ν_{M-C}

Clusters	ν_{M-C}, cm^{-1}	ν_{CO}, cm^{-1}	Solvent
$[Fe_3CoC(CO)_{12}]^-$ **(XI)**	800m, 760s	2066w, 2009s, 1992s, 1974m, 1940w sh	THF
$Fe_3CoRhC(CO)_{14}$ **(XII)**	788s, 780s sh, 765m sh	2102w, 2083w, 2063s, 2056s, 2049s, 2038w, 2029m, 2018m, 1995w, 1982w, 1970w, 1908w	C_5H_{12}
$Fe_3CoRhC(CO)_{13}PPh_3$ **(XIII)**		2075m, 2041s, 2027s, 2020m sh, 2006w, 1997m, 1975w, 1957w, 1857w	C_6H_{14}
$Fe_3CoAuC(CO)_{12}PPh_3$ **(XIV)**	796s,770m sh, 740s	2080m, 2034s, 2015s, 2005m, 1989m, 1970w, 1960m	C_5H_{12}
$Fe_3CoPdC(CO)_{12}C_3H_5$ **(XV)**	778, 757, 750	2080m, 2039s, 2018s, 2004m, 1991w, 1974w, 1963w	C_5H_{12}
$Fe_3CoPdC(CO)_{12}C_{10}H_{15}$ **(I)**		2075m, 2030s, 2013s, 2005m sh, 1986w, 1970w, 1950w	C_6H_{14}
$[Fe_3RhC(CO)_{12}]^-$ **(X)**		2074w, 2017s, 1979s, 1962m, 1944w sh	CH_2Cl_2
$Fe_3Rh_2C(CO)_{14}$	772, 760, 746	2075m, 2064s, 2055s, 2028m, 2020s, 1989m, 1910w	C_5H_{12}
$Fe_3RhAuC(CO)_{12}PPh_3$ **(XVI)**		2080w, 2035s sh, 2030s, 2005s sh, 2000m, 1985m, 1965m sh, 1950m	C_5H_{12}
$Fe_3RhPdC(CO)_{12}C_3H_5$ **(XVII)**		2080m, 2040s sh, 2030s, 2015s sh, 2010s, 1990s, 1970m sh, 1960m	C_5H_{12}
$Fe_3RhPdC(CO)_{12}C_{10}H_{15}$ **(II)**		2080m, 2045s sh, 2035s, 2015s sh, 2005s, 1990s, 1970m sh, 1955m	C_5H_{12}

Table 2
Parameters of X-ray measurements and crystal refinements for **XIV** and **XV**

Compound	**XIV**	**XV**
Molecular formula	$C_{31}H_{15}O_{12}AuCoFe_3P$	$C_{16}H_5O_{12}Co_3Fe_3Pd$
Molecular mass	$M = 1034$	$M = 722$
Crystal size	$0.1 \times 0.2 \times 0.2$ mm	$0.1 \times 0.2 \times 0.3$ mm
Crystal color	black	black
Absorption coefficient	6.14 mm^{-1}	3.58 mm^{-1}
Diffractometer	Syntex $P2_1$	Syntex $P2_1$
Temperature	−100°C	−100°C
Scanning method	$\theta/2\theta$	$\theta/2\theta$
Range of *hkl* measured	$-12 \le h \le 12$, $-14 \le k \le 15$, $0 \le l \le 16$	$0 \le h \le 12$, $0 \le k \le 15$, $0 \le l \le 36$
$2\theta_{max}$	54°	54°
Lattice	triclinic	orthorhombic
Space group	P-1	*Pbca*
Unit cell dimensions	$a = 11.039(3)$ Å, $b = 12.725(4)$ Å, $c = 13.647(4)$ Å, $\alpha = 79.00(3)°$, $\beta = 81.09(2)°$, $\gamma = 64.83(2)°$, $V = 1697(1)$ Å^3	$a = 10.878(1)$ Å, $b = 13.191(2)$ Å, $c = 30.214(3)$ Å, $\alpha = 90.00°$, $\beta = 90.00°$, $\gamma = 90.00°$, $V = 4336(1)$ Å^3
Z	2	8
Standard reflections	(1 4 0), (−2 −4 1) every 100 reflection, intensity variation < 2.8%	(0 0 8); (−4 2 0) every 100 reflection, intensity variation < 2.5%
Max/min residual electron density	1.77/−1.90 e/Å^3	0.73/−0.46 e/Å^3
F(000)	992	2784
P_{calc}	2.023 g/cm^3	2.109 g/cm^3
Measured reflections	5051	3676
Observed reflections ($I > 4\sigma I$)	4362	2573
R	0.041	0.038

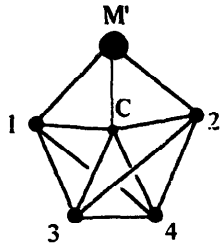

Fig. 1. The scheme of wing-tip butterfly cluster framework and probable sites for Co atom in the metal cores of **XIV** and **XV**.

the three electrode electrochemical microcell set inside the ESR spectrometer [17].

EXAFS spectra of **XV** for crystalline sample and its *o*-xylene solution (Pd K-edge) were measured on a synchrotron radiation of VEPP-3 electron storage ring (Novosibirsk) operating at the energy of 2.0 GeV with the electron current of 120 mA. Double crystal Si [111] monochromator was used, slightly detuned to reject higher harmonics. Data reduction and FT calculations were done in the Prof. Dmitry Kochubei group in the Institute of Catalysis, R.A.S. (Novosibirsk). Background was subtracted by polynomial fitting. Edge position was fixed at maximum of the first derivative of absorption curve. A Fourier transformation of $k^2\chi(k)$ with Gaussian window function was done in k range 3–12 $Å^{-1}$.

Absorption spectra of solutions of the compounds studied were recorded on a spectrophotometer Specord UV VIS; CD spectra were recorded on Jobin–Yvon Mark III dichrograph in a cell with the absorbing length ranging from 1.0 to 0.01 cm. The concentration of initial solutions was $\sim 1.10^{-3}$ mol/l.

2.12. Single crystal X-ray study of XIV and XV

X-ray data collection was done in the Centre for X-ray structural studies in the Institute of Organoelement Compounds of R.A.S. [3] Parameters of X-ray experiment and crystallographic data for $Fe_3CoAuC(CO)_{12}PPh_3$ (**XIV**) and $Fe_3CoPdC(CO)_{12}(\eta^3\text{-}C_3H_5)$ (**XV**) are shown in the Table 2. The structures were solved by direct methods and were refined by full-matrix least-squares using a PC version of SHELXTL [18]. Absorption correction was done with DIFABS. All non-hydrogen atoms were refined anisotropically. Hydrogen atoms were revealed in different Fourier map and were refined isotropically. The localization of Co atoms in the metal butterfly cores was performed on the last stages of refinement by comparison of R factors for the models with Co atom placed in each of four possible positions (Fig. 1) and for the model with Co atom randomly distributed over all positions (Table 3).

Table 3
Comparison of the R factors for different sites of Co atom in the metal frameworks of **XIV** and **XV**

XIV		XV	
Co atom site	R	Co atom site	R
none	0.0485	none	0.0388
1	0.0462	1	0.0402
2	0.0457	2	0.0399
3	0.0494	3	0.0397
4	0.0413	4	0.0382
1–4	0.0432	1–4	0.0387
1,2	0.0459	1,2	0.0397
3,4	0.0428	3,4	0.0385

2.13. Statistical analysis of geometry of pentanuclear clusters

A search for the structures of pentanuclear transition-metal carbide clusters in the Cambridge Structural Database (CSD) release of 1994 [19] (more than 126,000 structures) gives 54 clusters with $M_5(\mu_5\text{-}C)$ moiety (where M is any transition metal). All structures where carbon atom is bonded to exactly five transition metal atoms were included in the search quest. To characterize a geometry of carbide atom environment, interatomic distances M–C and bond angles M–C–M were calculated for each structure. A classification of cluster geometry to the structural types was done by the value of the next after the largest bond angle M–(μ_5-C)–M (see Section 3). The numbers of cluster valence electrons (CVE) in clusters extracted from CSD were determined from their molecular structure formulas.

3. Results and discussion

The method of the synthesis of heterometalllic carbidocarbonyl butterfly clusters by an attachment of a metal-containing fragment to $[Fe_3(CO)_9(\mu_3\text{-}CCO)]^{2-}$ dianion was developed by Kolis et al. [14]. A series of $[Fe_3MC(CO)_9L]^-$ butterflies (where M = Rh, Cu, Cr, Mn or W, and L is the ligand environment of M) [15,20,21] was obtained by this routine. According to the single crystal X-ray study of $[Fe_3RhC(CO)_{12}]^-$ (**X**), the heterometal atom M was localized in a basal position of the butterfly moiety. However, the closely related Co-containing butterfly cluster cannot be synthesized in this way because a substitution of Co atom for Fe atom in a triangular metal core takes place when $Co_2(CO)_8$ is used [21].

We have attempted therefore an alternative way to the synthesis of $[Fe_3CoC(CO)_{12}]^-$ anion. We exploited,

[3] Atomic coordinates and the full list of molecular geometrical parameters for **XIV** and **XV** are deposited in the Cambridge Structural Database.

after Tachikawa et al. [4], a consequent oxidative degradation of the cluster framework in the row octahedron → tetragonal pyramid → butterfly for a synthesis of heteropolymetallic carbidocarbonyl clusters. However, this method leads to the required species with the heterometal atom retained in the cluster core, but not in all cases.

The development of a direct method for the synthesis of heteropolymetallic carbidocarbonyl clusters requires the study of the applicability of other vertex elimination procedures, besides an oxidative degradation, to the initial octahedral cluster anion. Earlier we found [22] that a vertex elimination (called 'reductive degradation') takes place under the action of strong nucleophiles upon reductive conditions. Our data showed that the reductive degradation of the octahedral and tetragon–pyramidal heterometallic carbidocarbonyl clusters allowed to retain the heterometal atom in the cluster core during a stepwise decrease of nuclearity. The result obtained was not obvious because the stages of the electron addition/removal during electrochemical reduction of homometallic and heterometallic carbidocarbonyl clus-

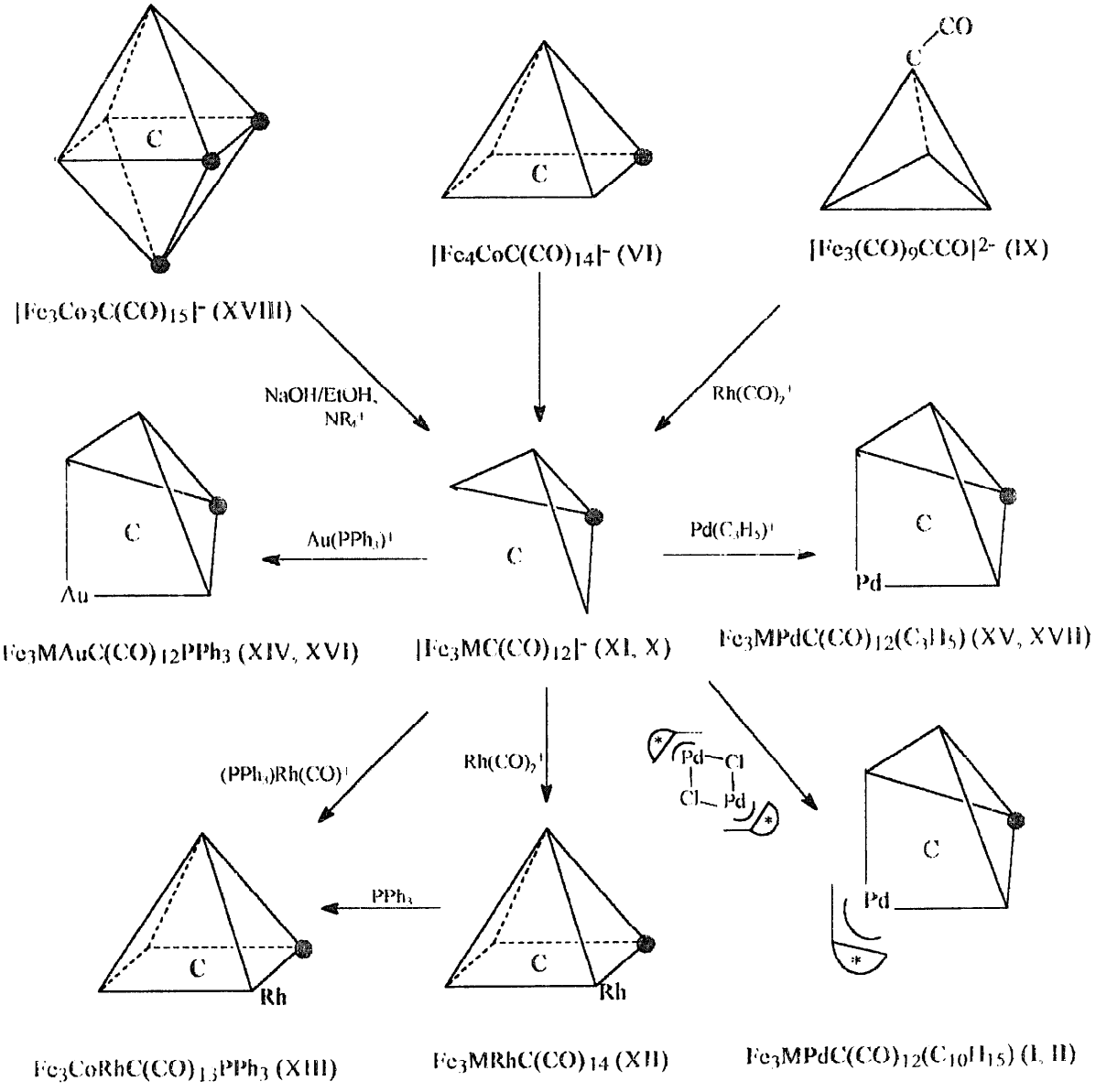

Scheme 2.

ters, unlike in the oxidative stages, are usually reversible [23].

The reaction of Co-containing clusters with KOH solution in ethanol appeared to be the best synthetic routine to heterometallic butterflies. It was found that stirring the hexanuclear anion $[Fe_3Co_3C(CO)_{15}]^-$ **(XVIII)** in the KOH/EtOH mixture for 10 min followed by a treatment with an excess of ammonium salt leads to a formation of the $[Fe_3CoC(CO)_{12}]^-$ anion **(XI)** (Scheme 2). Noteworthy was that the yield of the main product was very sensitive to small changes in reaction conditions, varying from 10% to 40–45%. When the pentanuclear anion $[Fe_4CoC(CO)_{14}]^-$ **(VI)** was treated in a similar way, the same cluster **XI** was formed. For the latter reaction, in some cases, it was possible to isolate the hexanuclear monoanion **I** and the tetranuclear homometallic dianion $[Fe_4C(CO)_{13}]^{2-}$ as by-products.

IR pattern of **XI** obtained by this method was identical to that of the butterfly $[Fe_3RhC(CO)_{12}]^-$ **(X)** with the known X-ray structure [16] both in band positions and their intensities. It allowed us to suggest that the **XI** is also a heterometallic butterfly with μ_4-C carbide atom. Along with the chemical analysis data, the presence of Co atom correlates with the diamagnetism of **XI** monoanoin (requiring at least one atom with odd number of valence electrons).

Single crystal X-ray study of the clusters obtained by the addition of heterometallic vertices to **XI** (vide infra) demonstrated that two $[Fe_3MC(CO)_{12}]^-$ butterflies with M = Rh **(X)** and Co **(XI)** are isostructural. The basal position of the heterometal atom in the butterfly moiety of **X** was proved by single crystal X-ray data. The indirect determination of the Co atom site in **XI** also gives a basal position. Nevertheless, our data do not exclude the possibility of structural rearrangement of the $Fe_3M(C)$ butterfly with a migration of the M atom between two stereochemically non-equivalent positions.

The carbide monoanion **XI** undergoes the organic reactions typical for that type of compounds giving noncharged 'organic' adducts to the μ_4-C atom.

3.1. Electrochemical reduction of XI

Anion radical $\{[Fe_3Co_3C(CO)_{15}]^-\}^-$ obtained via electrochemical reduction of **XVIII** ($E_{gen} = -0.5$ V) in acetonitrile at 253 K displays eight lines in ESR spectrum ($g = 2.015$, $A_{Co} = 42$) (Fig. 2). Generation at the potential of the second wave limiting current leads to a disappearance of the ESR signal. The values of g and A_{Co} are close to the corresponding parameters for well known Co_3C-containing compounds although in our case the unpaired electron interacts with only one Co atom instead of three. That fact supports a suggestion that the initial product of the cathode reduction rapidly eliminates a diamagnetic binuclear Co_2 fragment with a certain number of CO ligands:

$$[Fe_3Co_3C(CO)_{15}]^- + e^- \rightarrow \{[Fe_3Co_3C(CO)_{15}]^-\}^-.$$

$$\{[Fe_3Co_3C(CO)_{15}]^-\}^- \rightarrow \{[Fe_3CoC(CO)_{15-n}]^-\}^- + Co_2(CO)_n(CH_3CN)_m$$

After the removal of extra electrons and probably CO ligands the initial unstable paramagnetic particle $\{[Fe_3CoC(CO)_{15-n}]^-\}^-$ turns into the stable anion $[Fe_3CoC(CO)_{12}]^-$ **(XI)**. This suggestion agrees well with our data on the reductive degradation of cluster frameworks (vide supra). The main direction of degradation of **XVIII** and **VI** is an elimination of one or two atoms from the metal core: the intermediate product with one Co atom is stabilized as the anion **XI**.

3.2. Two directions of addition of M-containing groups to heterometallic butterflies $[Fe_3MC(CO)_{12}]^-$ with M = Co (XI) and Rh (X)

3.2.1. Interaction of XI and X with M-containing reagent, where M = Co, Rh

$[Rh(CO)_2Cl]_2$ **(IV)** is a typical reagent for adding a new vertex to a *nido*-polyhedron. The interaction of **IV** with **XI** butterfly goes easily resulting in a formation of the square pyramidal cluster $Fe_3CoRhC(CO)_{14}$ **(XII)** with a good yield. The noncharged heterometallic cluster **XII** most probably contains the Rh and Co atoms in the base of the pyramid linked via bridging CO ligand [24]. Element analysis data and IR spectra in the region of ν(C–O) and ν(M–C) for **XII** are identical to those of the sample of the known cluster with the same formula that we obtained earlier by the alternative method [25].

Fig. 2. ESR spectrum of anion-radical obtained in electrochemical reduction of **XVIII** at $E_{gen} = -1.30$ V. Pt electrode in MeCN, 0.1 M Et_4NBF_4 related to Ag, $c = 10^{-3}$ mol/l at 293 K.

There are five stereochemically nonequivalent sites for an attack of PPh_3 ligand in the asymmetric $Fe_3CoRhC(CO)_{14}$ molecule: $Fe(CO)_3$ group in the apex, two approximately equivalent basal Fe atoms, and the basal Co and Rh atoms linked by the bridging CO ligand. *A priori* one can suggest that the presence of bridging CO ligand between Co and Rh atoms makes this part of the molecule the most preferential to a nucleophilic attack. We have found that the CO substitution readily goes under excess of PPh_3 at room temperature giving only one product with 50% yield. Besides the more common methods (element analysis and IR), the product of the substitution was characterized by ^{252}Cf-plasma desorption mass-spectrometry (PDMS) [26]. The molecular ion ($m/z = 967.8$) and the fragmentation pattern ($m/z = 883.5$, 856.7, 828.0, 799.3, 771.1, 743.4, 716.0, 685.4 and 630.5) correspond to a consequent detachment of 3, 4, 5, 6, 7, 8, 9 and 12 CO groups from the ligand environment.

These data unequivocally confirm that, in spite of a large excess of PPh_3, only the product of the ligand monosubstitution was formed. To determine the coordination site of PPh_3 ligand, we performed the head-on synthesis of the monosubstituted $Fe_3CoRhC(CO)_{13}PPh_3$ (**XIII**). Reaction of mononuclear $[RhCl(PPh_3)_2(CO)]$ (**V**) with the butterfly **IX** gave the only product **XIII** that is identical to the compound prepared via reaction (1) (Scheme 2). The structure of **XIII** was determined earlier by single crystal X-ray study [24]. A tetragon–pyramidal structure of the cluster core in heterotrimetallic **XII** cluster is thus reliably confirmed.

Similar to the addition of the Co vertex to the $Fe_3Co(C)$ butterfly core in **XI**, an interaction of **XI** with $Co_2(CO)_8$ gives the known uncharged $Fe_3Co_2C(CO)_{14}$ cluster [27]. Furthermore, the closely related $Fe_3Rh(C)$ butterfly framework in **X** readily adds another $Rh(CO)_n^+$ vertex giving the known uncharged $Fe_3Rh_2C(CO)_{14}$ cluster with tetragon–pyramidal geometry [27,28]. A uniform reaction pathway for $M(CO)_n^+$ addition to heterometallic butterflies $[Fe_3MC(CO)_{12}]^-$ (M = Co, Rh) evidently lies through a formation of uncharged tetragon–pyramidal species.

3.2.2. Addition of $AuPPh_3^+$ and $Pd(\eta^3\text{-}C_3H_5)^+$ units to heterometallic $[Fe_3MC(CO)_{12}]^-$ clusters

According to Tachikawa et al. [4] and our recent studies, the addition of metal-containing fragments to both homometallic and heterometallic tetragonal pyramids gives only octahedral clusters independent of the nature of metal atom and their ligand environment. In particular, the Pd, Pt, and Au atoms did not differ considerably from other metals.

A dependence of structure of clusters obtained in reactions of addition to heterometallic butterflies on a nature of metal in the metal-containing fragment was demonstrated for the first time in this work. We found

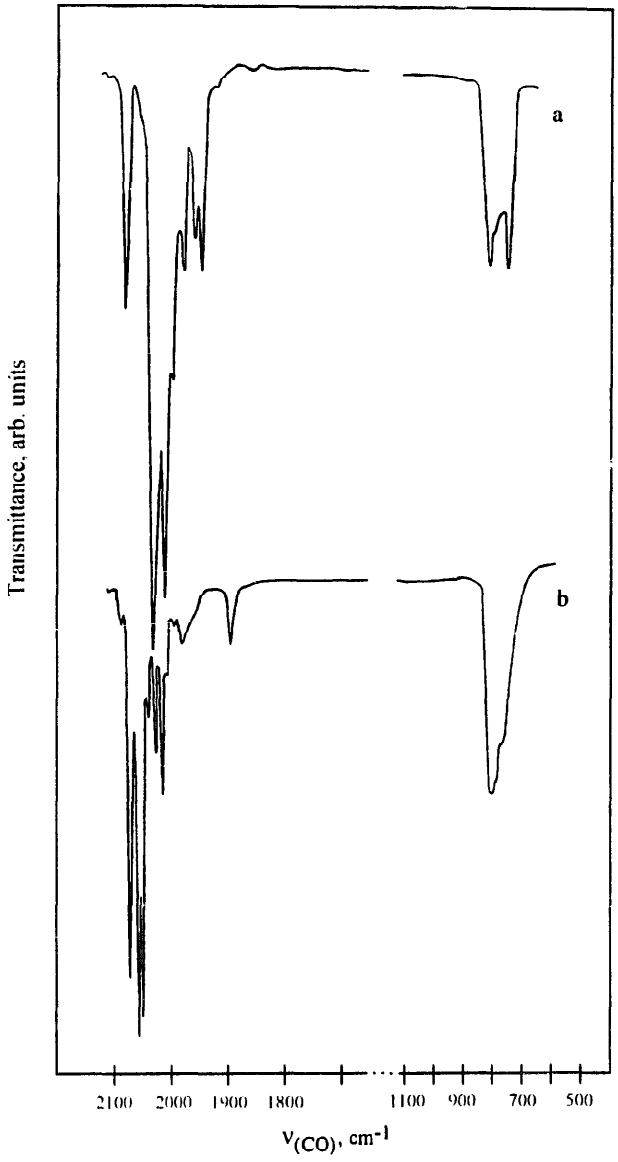

Fig. 3. Comparison of IR spectra of **XIV** (a) and **XII** (b) in the region of ν_{C-O} and ν_{M-C}.

that the addition of $AuPPh_3^+$ instead of isoelectronic $Rh(CO)_2^+$ to **XI** leads also to a formation of the uncharged cluster $Fe_3CoAuC(CO)_{12}PPh_3$ (**XIV**). However, IR spectrum of **XIV** differed significantly from the corresponding spectra of Rh derivative **XII** and of the other known homometallic and heterometallic tetragon–pyramidal carbidocarbonyl clusters by positions and shapes of both ν_{CO} and ν_{M-C} bands (see Fig. 3). The single crystal X-ray study of **XIV** revealed an alternative wing-tip butterfly structure of its metal core; it was the first example of uncharged heterotrimetallic cluster of this geometry.

$[Pd(\eta^3\text{-}C_3H_5)Cl]_2$ (**VIII**) reacts with the **XI** in a similar way giving the uncharged cluster $Fe_3CoPdC(CO)_{12}(\eta^3\text{-}C_3H_5)$ (**XV**). Analogous to **XIV**, the IR spectrum of **XV** differs significantly from that of

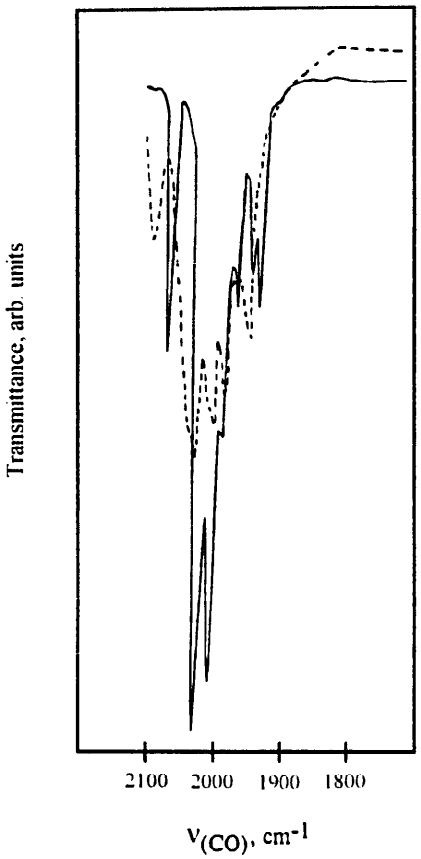

Fig. 4. Comparison of IR spectra of **XIV** (————) and **XVI** (– – –) in the region of ν_{C-O}.

XII. The single crystal X-ray study of **XV** showed that the cluster core has a wing-tip geometry with the Pd(η^3-C_3H_5) fragment attached to the butterfly moiety without substantial structural changes (see Section 3.3).

To compare the reactivity of the different heterometallic clusters, we studied a possibility of the addition of the same groups $Rh(CO)_2^+$, $AuPPh_3^+$ and Pd(η^3-C_3H_5)$^+$ to the butterfly cluster $[Fe_3RhC(CO)_{12}]^-$ (**X**) obtained by the Shriver's method. We found that the Rh-containing butterfly reacts with $AuPPh_3^+$ and Pd(η^3-C_3H_5)$^+$ in a way similar to the Co analog giving the soluble (in pentane and hexane) species $Fe_3RhXC(CO)_{12}$, where X = $AuPPh_3$ (**XIV**) or Pd(η^3-C_3H_5) (**XV**). The IR spectra of **XIV** and **XV** resemble those of the corresponding uncharged Co analog by positions, numbers and relative intensities of the bands (Fig. 4). One can suggest that the **XIV** and **XV** clusters have the same wing-tip butterfly geometry of metal cores differing from the Co analog only by the presence of Rh atom instead of Co atom in the basal position within the butterfly moiety.

So we have found that the addition of metal-containing fragments to heterometallic butterfly **XI** proceeds by two principal directions: the route A results in a formation of tetragonal pyramid while the route B results in a formation of wing-tip butterfly (see Scheme 1). It should be noted that both types of clusters obtained have cluster valence electrons (CVE) of 74.

Wing-tip butterfly clusters are well known; there were more than 20 crystal structures done for these species. The usual approach to their synthesis consists in the addition of nucleophile to tetragon pyramidal clusters [29]. The clusters reported in this work do not differ significantly (besides CVE-number) from the analogs described in the literature. It is important, however, that the way of the vertex addition is typical only for noble metals with a preferable low-coordination ligand configuration: linear (for Au) or planar (for Pd). The addition of the metal atoms with a preferable octahedral coordination to the same heterometallic butterflies also gives 74-electron species but with another, i.e., tetragonal pyramidal geometry of the metal core.

In **XII** and **XIII** obtained by the addition of 12-electron cation $Rh(CO)_2^+$ to the butterfly core, the Rh atom in a base of the tetragonal pyramid has a distorted octahedral environment. The isoelectronic Pd(η^3-C_3H_5)$^+$ and $AuPPh_3^+$ fragments can either enter into a base of pyramid and expand the metal atom's coordination to the octahedral one or retain the low coordination number in a wing-tip butterfly geometry. In practice, the second possibility takes place. Mononuclear bridging fragments ML_n with the unfilled coordination sphere of M atom link the wing positions of $Fe_3Co(C)$ butterfly moiety by the metal–metal bonds. The linking *exo*-heterometal atom M (for M = Pd and Au) probably is not included into the delocalized electron system of the butterfly framework and retains its particular electronic and steric configuration [29].

3.3. Structural study

The molecular structures of **XIV** and **XV** according to the single crystal X-ray data are shown in Figs. 5 and 6, respectively. The main interatomic distances and bond angles therein are shown in Table 4. In a wing-tip butterfly metal core of both clusters, three Fe atoms and one Co atom form a butterfly moiety with Fe atoms in wing positions linked through Au or Pd bridges in **XIV** and **XV**, respectively. According to the refinement data (see Table 3), the Co atom is placed in the basal position of the butterfly. Each Co and Fe atom has three terminal CO ligands. The Au atom in **XIV** is coordinated by the PPh_3 and the Pd atom in **XV** is coordinated by the η^3-allyl ligand.

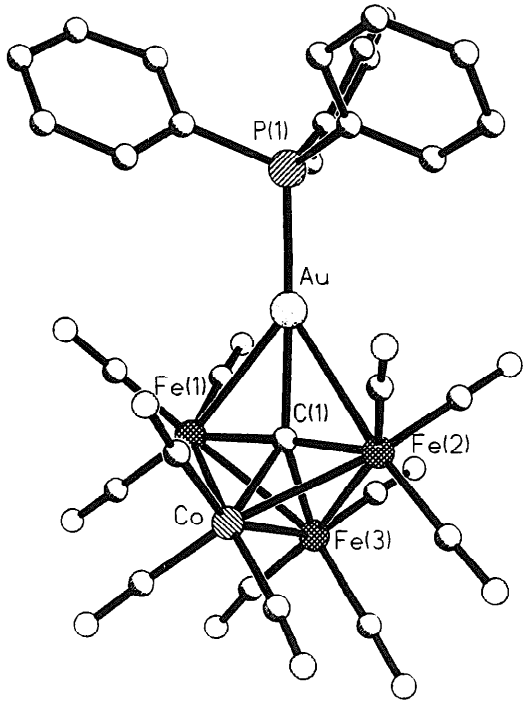

Fig. 5. Structure of **XIV**.

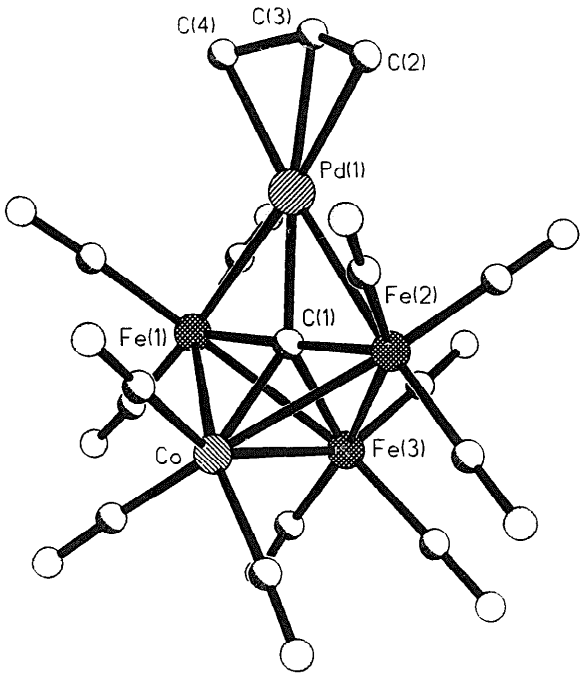

Fig. 6. Structure of **XV**.

Table 4
Main interatomic distances and bond angles in **XIV** and **XV**

XIV		**XV**	
Interatomic distance	*d*, Å	Interatomic distance	*d*, Å
Au–Fe(1)	2.878(2)	Pd–Fe(1)	2.694(1)
Au–Fe(2)	2.812(2)	Pd–Fe(2)	2.6854(9)
Fe(1)–Fe(3)	2.618(2)	Fe(1)–Fe(3)	2.658(1)
Fe(1)–Co	2.617(2)	Fe(1)–Co	2.656(1)
Fe(2)–Fe(3)	2.630(2)	Fe(2)–Fe(3)	2.653(1)
Fe(2)–Co	2.635(2)	Fe(2)–Co	2.653(1)
Fe(3)–Co	2.518(2)	Fe(3)–Co	2.521(1)
Au–C(1)	2.10(1)	Pd–C(1)	2.005(6)
Fe(1)–C(1)	1.86(1)	Fe(1)–C(1)	1.817(6)
Fe(2)–C(1)	1.84(1)	Fe(2)–C(1)	1.831(6)
Fe(3)–C(1)	1.91(1)	Fe(3)–C(1)	1.895(6)
Co–C(1)	1.93(1)	Co–C(1)	1.924(6)
Au–P	2.274(3)	Pd–C(allyl)	2.11–2.15
Fe–C(CO)	1.78–1.84	Fe–C(CO)	1.77–1.81
Co–C(CO)	1.77–1.81	Co–C(CO)	1.78–1.82
Fe(3) · · · Au	3.873	Fe(3) · · · Pd	3.692
Co · · · Au	3.625	Co · · · Pd	3.631
Bond angle	φ, deg	Bond angle	φ, deg
Fe(1)–C(1)–Au	93.1(5)	Fe(1)–C(1)–Pd	89.5(3)
Fe(1)–C(1)–Fe(3)	88.1(5)	Fe(1)–C(1)–Fe(3)	91.5(3)
Fe(1)–C(1)–Co	87.5(5)	Fe(1)–C(1)–Co	89.4(3)
Fe(2)–C(1)–Au	90.9(5)	Fe(2)–C(1)–Pd	88.7(2)
Fe(2)–C(1)–Fe(3)	89.3(5)	Fe(2)–C(1)–Fe(3)	90.8(3)
Fe(2)–C(1)–Co	88.8(5)	Fe(2)–C(1)–Co	89.9(3)
Fe(3)–C(1)–Co	82.1(5)	Fe(3)–C(1)–Co	82.6(2)
Fe(1)–C(1)–Fe(2)	175.8(7)	Fe(1)–C(1)–Fe(2)	177.7(4)
Au–C(1)–Fe(3)	149.9(6)	Pd–C(1)–Fe(3)	142.4(3)
Au–C(1)–Co	128.1(5)	Pd–C(1)–Co	135.0(3)

3.3.1. Cluster $Fe_3CoAuC(CO)_{12}PPh_3$ (XIV) [4]

Wing-tip butterfly **XIV** forms molecular crystals with the normal van der Waals intermolecular contacts. The M–CO bond lengths (where M = Fe or Co) have the common values of 1.77–1.78(1) Å. The bond angles Fe(1)–C(1)–Fe(2) in **XIV** and **XV** (between Fe atoms in axial positions) are close to 180°; the Fe(3), Co, and Au atoms are situated approximately in the one plane with carbide C(1) atom (the sum of the corresponding angles at carbide atom is 360° for **XIV** and 359.9° for **XV**). Carbide atom thus has a distorted trigonal bipyramidal environment of five metal atoms with noticeable difference in the values of bond angles Au–C(1)–Co and Au–C(1)–Fe(3) [128.1(5)° and 149.9(6)° respectively]. As a consequence, the corresponding intramolecular nonbonded contacts Au · · · Co (3.625 Å) and Au · · · Fe(3) (3.873 Å) differ significantly and the geometry of the metal core deviates from the ideal C_{2v} to C_s symmetry. The bond length Au–P (2.274(1) Å) and other geometrical parameters of the ligand environment of cluster **XIV** are in agreement with the known structural data.

The geometry of $M_4Au(C)$ moiety similar to that found in **XIV** was observed earlier in the structure of heterodimetallic cluster $Fe_4AuC(\mu\text{-H})(CO)_{12}PPh_3$ prepared in the reaction of tetrahedral anion $[Fe_4(CO)_{13}]^{2-}$ and $AuPPh_3Cl$ with 47% yield [32].

3.3.2. Structure of $Fe_3CoPdC(CO)_{12}(\eta^3\text{-}C_3H_5)$ (XV)

Similar to **XIV**, the **XV** cluster forms molecular crystals without any unusually short intermolecular contact. Most bond distances and bond angles in **XV** have their typical values. The environment of carbide C atom in the wing-tip butterfly **XV** is also a distorted trigonal bipyramid, although the deviations from the ideal C_{2v} geometry of the $Fe_3CoPd(C)$ framework are less pronounced as compared to **XIV**. Intramolecular nonbonded contacts Pd · · · Co 3.631 and Pd · · · Fe(3) 3.692 Å are relatively close and the difference between bond angles Pd–C–Fe(3) (142.4(3)°) and Pd–C–Co (135.0(3)°) is only 7.4° (21.8° in **XIV**, see Table 4).

Table 5
Geometrical parameters of Pd(η^3-allyl) fragment in **XV** in comparison with (β-pinenyl)Pd(Me_2bpy)

Bond lengths (Å) and bond angle (°) in Pd(η^3-allyl)	XV	(β-pinenyl)-Pd(Me_2bpy) [32,33] (two independent molecules)	
Pd–C(1)	2.146(7)	2.15	2.21
Pd–C(2)	2.109(8)	2.21	2.16
Pd–C(3)	2.151(7)	2.18	2.10
C(1)–C(2)	1.30(1)	1.47	1.36
C(2)–C(3)	1.30(1)	1.36	1.41
C(1)–C(2)–C(3)	135(1)	112	122

The bond lengths and angles of Pd(η^3-C_3H_5) fragment in **XV** are close to the corresponding values in the mononuclear *o*-methylbipyridyl Pd complex with η^3-pinenyl ligand [32,33] (Table 5). A noticeable difference in the values of C(1)–C(2)–C(3) angle at the central atom of allyl ligand can be caused either by an electron donor influence of hydrocarbon periphery of a pinene ligand or by some disordering of the η^3-ligand. The data in Table 5 support the suggestion (see above) that the mononuclear [(η^3-allyl)Pd] fragment enters into wing-tip butterfly framework without significant changes in its electronic and geometrical structure.

3.3.3. Statistical analysis of $M_5(\mu_5\text{-}C)$ cluster geometry with CSD

The 54 structures extracted from CSD (see Section 2), together with the **XIV** and **XV** structures, were used in a statistical analysis. Metal atoms in moieties $M_5(\mu_5\text{-}C)$ were enumerated as in the Fig. 7. The angle M–C–M at the central carbide atom, closest to 180°, was assigned as 1–C–2. The rest of the M atoms disposed in the plane perpendicular to 1–C–2 axis were numbered 3, 4 and 5 so that the maximal angle formed by these vertices was 3–C–5.

The 3–C–5 bond angle appeared to be a key parameter in the classification of the wing-tip butterfly structures. All pentanuclear carbide clusters can be subdivided into three main geometrical types: trigonal bipyramid (TB), wing-tip butterfly (WTB) and square pyramid (P). For ideal TB geometry, the 3–C–4, 3–C–5 and 4–C–5 angles are equal to 120°. In the case of WTB, one of the angles (ca. 80°) is significantly less than the two others (ca. 140°) and, for P geometry, the 3–C–5 angle is equal to 180° as the two others are equal to 90°. The diagram of the 3–C–5 bond angle in the dependence on both geometry type and number of cluster

[4] The very closely related cluster with the same stoichiometry $(Ph_3PAu)Fe_3Co(CO)_{12}(\mu_5\text{-}C)$ (**XIVa**) was independently obtained as a by-product wi with a very low yield and was structurally studied by Thone and Vahrenkamp [30]. The structure of **XIVa** differs from **XIV** only by a position of the Co atom in the metal core (wing instead of basal position of wing-tip butterfly moiety). The different color of the obtained species (red for **XIVa** and black for **XIV**) and the difference in their IR spectra point to the isomeric structures. The structural parameters of both triclinic P-1 crystals are quite similar [a = 11.095(2), b = 12.797(3), c = 13.721(3) Å, α = 79.54(3)°, β = 81.49(3)°, γ = 64.73(3)° for **XIVa** and a = 11.039(2), b = 12.725(3), c = 13.647(4)Å, α = 79.00(2)°, β = 81.09(2)°, γ = 64.83(2)° for **XIV**] taking into account the different temperatures of their X-ray studies (room temperature for **XIVa** and −100°C for **XIV**). Atomic positions and interatomic distances in these structures are practically identical (the maximum deviation in the corresponding intermolecular contacts in **XIV** and **XIVa** is less than 0.04 Å). Unfortunately, the procedure of Co atom localization was not described in Ref. [31] which does not allow to prove or reject the suggestion on identity of **XIV** and **XIVa**. However, according to Vahrenkamp (H. Vahrenkamp, personal communication), these clusters are most likely to be identical.

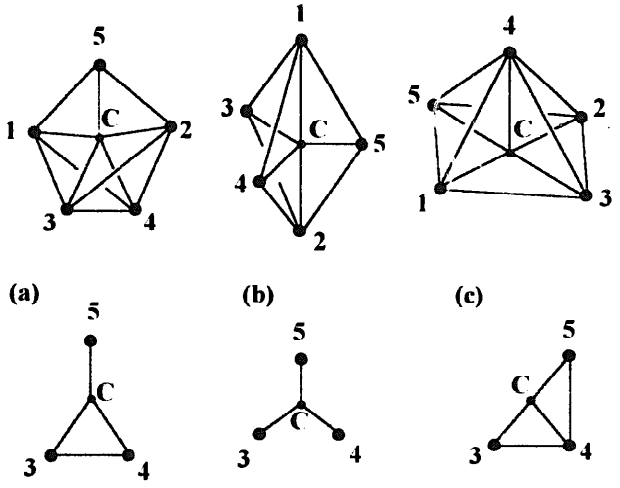

Fig. 7. Types of geometry of the pentanuclear carbide clusters and projections of the coordination polyhedra of the carbide atom to the plane perpendicular to 1–C–2 axis: (a) wing-tip butterfly (WTB), (b) trigonal bipyramid (TB), (c) square pyramid (P).

valence electrons for all of 56 structures is shown in Fig. 8.

Cluster geometries in the diagram correspond to rather continuous distribution between main TB, WTB and P structural classes. An analysis of other angles showed that the deviations from ideal C_{2v} geometry observed for **XIV** and **XV** are typical for clusters having the WTB metal core with two equivalent basal positions of butterfly moiety. No correlation between the deviations and the number of cluster valence electrons was detected. Presumably, these distortions reflect a balance of weak interatomic interactions including the influence of crystal packing.

It is noticeable that WTB and P structural types are observed for all even numbers of CVE in the range of 72–76. However, the CVE number of 76 is predominant for WTB clusters and the CVE number of 74 is predominant for P clusters (see Fig. 8). Both predominant numbers are 'magic' according to Wade's rule for clusters with two and one open faces, respectively [34]. This fact is in agreement with the earlier observed statistical character of the rules for magic numbers of CVE in small transition metal clusters [35]. So far, the fact is that the CVE number of 74 for **XIV** and **XV** among WTB clusters represents an apparent exception from the general rule.

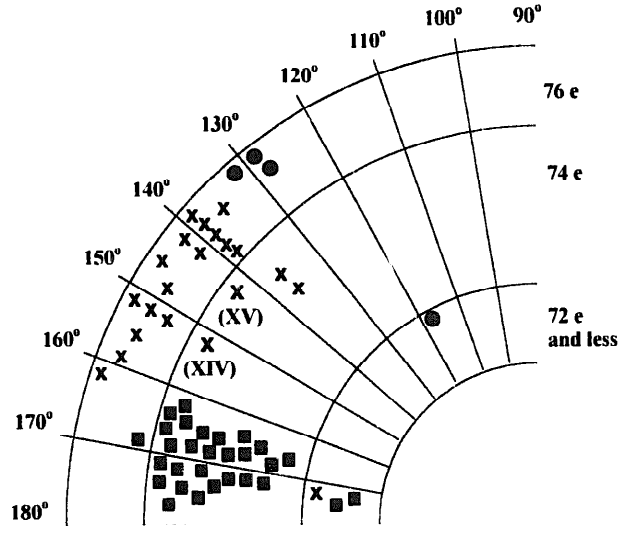

Fig. 8. Distribution of the 3–C–5 bond angle in the pentanuclear carbide clusters from CSD data: squares denote square pyramids; x for wing-tip butterflies; and circles for trigonal bipyramid.

In fact, as it was shown in Ref. [29], the bridging metal atom in wing-tip butterfly clusters (as well as in **XIV** and **XV**) should be considered as *exo*-fragment relative to butterfly moiety. The difference of 76-electron WTB species from 74-electron clusters **XIV** and **XV** consists in that the metal *exo*-atoms have a coordination number of 6 and the filled 18-electron shell for the former group and the unfilled 16-electron shell with the nonuniform (almost planar) coordination environment in the latter.

Statistical treatment of CSD data revealed the possibility of structural rearrangement and flexibility of the cluster core in wing-tip butterfly.

3.3.4. *Structure of XV in a solution*

To study the possible rearrangements of the $Fe_3CoPd(C)$ framework, the EXAFS study of **XV** samples in solid state and *o*-xylene solution was performed. The Fourier transforms (FT) of Pd K-edge EXAFS spectra for both samples (Fig. 9) consist of three distinct

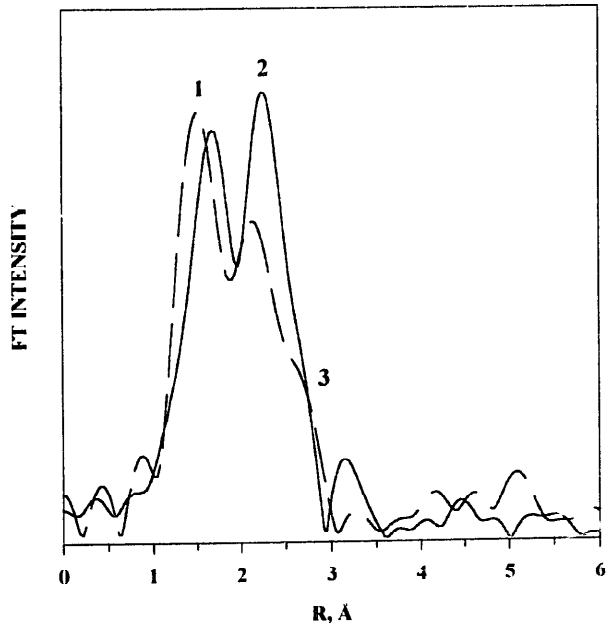

Fig. 9. Fourier transforms (FT) of EXAFS spectra for **XV** (Pd K-edge) in the solid sample (solid line) and in the *o*-xylene solution (dashed line). The three closest coordination spheres of Pd atom are indicated by numbers.

maxima corresponding to the (1) nearest surrounding of Pd atom [Pd–C(μ_5-C, allyl)], (2) metal–metal Pd–Fe bonds with atoms in wing positions and (3) non-bonded contacts [Pd · · · (Fe, Co)] with atoms in basal positions (as a shoulder for the solid sample). However, the peak intensities for the sample in a solution are diminished and the second and third coordination spheres are closer to each other than in crystalline **XV**.

EXAFS data for **XV** therefore suggest a structural flexibility of the $Fe_3CoPd(C)$ framework in a solution. The decrease in intensity and broadening of the maxima corresponding to Pd-metal contacts may reflect fluctuations of the Pd(allyl) unit within a coordination sphere of the interstitial (μ_5-C) atom. A flexibility of the wing-tip butterfly metal core agrees with the observed deviations of **XIV** and **XV** structures from C_{2v} symmetry as well as with the broad range of the cluster geometric parameters from CSD data (vide infra).

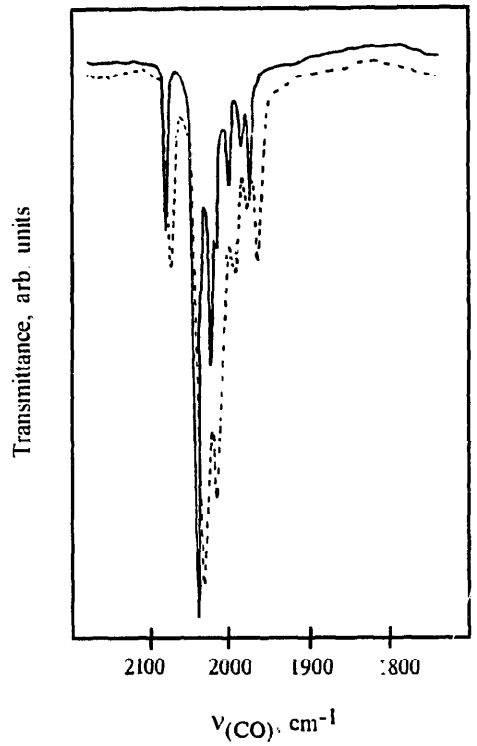

Fig. 10. Comparison of IR spectra of **XV** (————) and **I** (– – –) in the region of ν_{C-O}.

4. Optically active heterotrimetallic wing-tip butterflies

4.1. Synthesis of optically active wing-tip butterflies $Fe_3MPdC(CO)_{12}(\eta^3\text{-}C_{10}H_{15})$ (M = Co, Rh)

Square pyramidal heterotrimetallic cores of carbide clusters with two different heterometal atoms in basal *cis*-positions are chiral, since they have no symmetry elements. Contrary to them, even the heterotrimetallic members of the wing-tip butterfly family with a heterometal atom in the wing-bridging site are achiral because of the symmetry plane passing through the carbide C atom and two heterometal atoms. However, an introduction of the asymmetrically substituted allyl ligand to the bridging Pd atom in **XV** and **XVI** opens a way to the chiral wing-tip butterfly derivatives.

Binuclear optically active (η^3-allyl) Pd complex derived from the natural β-pinene $C_{10}H_{16}$, with a high degree of optical purity was obtained and reliably characterized in Ref. [13]. We reproduced the synthesis and prepared the complex [(β-$C_{10}H_{15}$)$PdCl]_2$ (**III**) by interaction of Na_2PdCl_4 with β-pinene ($[\alpha]_D = -19.7°$). Optical rotation of the prepared compound ($[\alpha]_D = +25°$, $c = 6.024$ g/100 ml; $CHCl_3$, $d = 1$ cm) agrees well with the reported data [13].

The uncharged optically active clusters $Fe_3MPdC(CO)_{12}(\eta^3\text{-}C_{10}H_{15})$ where M = Co (**I**) and Rh (**II**) were prepared via interaction of **III** (as a donor of the chiral metal-allyl moiety) with **XI** and **X**, respectively (see Section 2). Clusters **I** and **II** are dark brown substances, soluble in hexane and CH_2Cl_2. Their IR spectra in the region of ν_{CO} are almost identical to the corresponding spectra of **XV** and **XVII** (Fig. 10, Table 1). One may thus suggest that the clusters with the η^3-(β-pinenyl) ligand have a geometry similar to that of the corresponding η^3-allyl analog (Fig. 11).

The η^3-coordination of β-pinene to Pd atom obviously results in a formation of planar chirality in the substituted Pd(π-allyl) fragment in addition to two asymmetric carbon atoms of the initial β-pinene. However, the incorporation of the (β-$C_{10}H_{15}$)Pd moiety into the wing-tip butterfly framework does not create any additional asymmetry, thus retaining the achiral pentanuclear metal core (see above).

In accordance with the reported single crystal X-ray structures [32,33], the formation of the less sterically crowded isomers with *anti*-orientation of Pd atom and the bulky CMe_2 group of β-pinenyl ligand may be suggested for **I–III** (see Fig. 11). We assume the retaining of the initial (−)-(1S, 5S)-β-pinene absolute configuration in the complexes, which gives for the mononuclear fragment Pd(β-pinenyl) the absolute configuration (1R, 2S, 3S, 5R) following the nomenclature of Cahn et al. [36] or (1R, 5R, R_{pl}) following the system of Schlogl et al. [37] and Marguarding et al. [38].

4.2. Analysis of absoption and circular dichroism spectra of I–III

The chiroptical properties of the following heterometallic clusters with up to three different transition metal atoms in a polyhedron were studied to date:

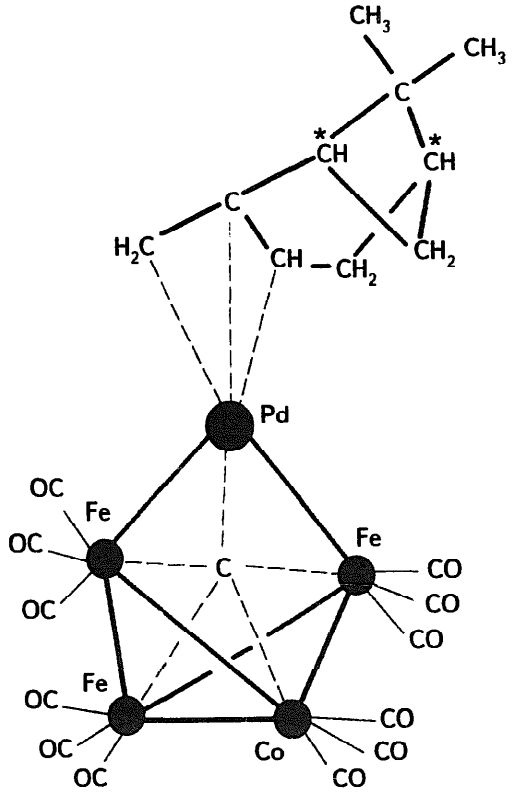

Fig. 11. Model of the molecular structure of **I** based on the X-ray molecular structures of **XV** (our data) and $[Pd(\eta^3\text{-}C_{10}H_{15})\{S(-)BINAP\}](CF_3SO_3)$ [32].

$XFe(CO)_3Co(CO)_3MCp(CO)_2$ (where X = S, M = Cr, Mo, or W [39,40], and X = PR, M = Mo or W [41]), $RCCo(CO)_3NiCpMCp(CO)_2$ (where M = Mo or W [42]), $Os_3(\mu_2\text{-}H)(CO)_n(\mu_2\text{-}Y)$ [where $n = 10$, Y = CO(NHR) or py [43–45]; $n = 9$, $Y=O\overline{CHCH_2CH(COOR)NHCH_2}$)].

$(\mu_3\text{-}CCH_3)Co_3(CO)_6(Ph_2PCH_2P(CH_3)_2)L'$ (where L' is a chiral phosphine ligand [46]), $(\mu_3\text{-}S)MoCpCo_2(CO)_6$ [47], and $Ni_2Cp(Cp')C_2RR'$ (where Cp' is a substituted cyclopentadienyl ligand [48]). CD spectra which are most suitable for a theoretical analysis of optical activity were studied only for few of these clusters [40,43,44,47,48]. For some other clusters, optical rotatory dispersion was measured [39–41,46], and only the optical rotation data at several wavelengths were reported for the remaining species [40–42]. To our knowledge, chiral tetrahedral clusters containing four different transition metal atoms were never prepared in an optically active form (see Ref. [39] and references therein).

η^3-Allyl complexes of Pd^{2+} are widely used in synthesis and catalysis including asymmetric ones [49,50]. Nevertheless, studies of correlations between stereochemistry and optical activity started in the early 1970s still are not much developed. Our recent results on the optical activity of palladium β-pinene derivatives of a known stereochemistry briefly reported earlier [2,6] are therefore important.

Table 6
AB and CD spectra of the $[Pd(\eta^3\text{-}C_{10}H_{15})Cl]_2$ (**III**) in CH_2Cl_2 solution

AB		CD		Band	CD [51]	
ν, kK	ε	ν, kK	$\Delta\varepsilon$		ν, kK	$\Delta\varepsilon$
18.50sh	5	17.86sh	−0.002	A		
		23.81	−0.060	B	23.75	−0.021
		26.88	+0.527	C		
29.50	1903	29.94	+1.0	D	28.99	+0.735
		34.96	−0.064	E		
> 37.0	> 3000	> 35.7	+CE	F	42.37	+10.61

4.2.1. Chiroptical properties of III

For **III** in CH_2Cl_2 solution, CD data were reinvestigated and the absorption spectrum was measured (Table 6, Fig. 12). The analysis of CD spectrum of **III** was performed in the framework of one-electron model of optical activity [3,52,53]. To our knowledge, this approach was not applied earlier for transition metal π-allyl complexes.

Table 6 demonstrates that the electron transitions in the CD spectrum of **III** are better resolved than in its

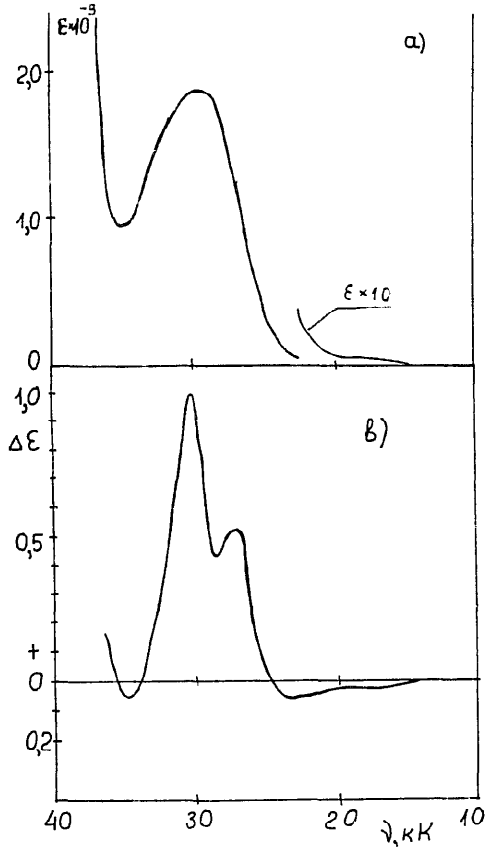

Fig. 12. AB (a) and CD (b) spectra of the complex **III**.

Table 7
Absorption spectra of the **XI**, **XV**, and **I** in CH_2Cl_2 solution

XI		**XV**		**I**	
ν, kK	ε	ν, kK	ε	ν, kK	ε
16.0 inflat	1190	18.2sh	1345	17.50 inflat	2210
20.0	3890	21.0sh	1965	20.0sh	3316
		27.2 inflat	6069		
29.0sh	7840	32.2sh	16,667	31.0sh	21,056
36.0sh	21,940	38.0sh	28,410	36.5sh	29,215

AB spectrum. Our CD data revealed more Cotton's effects (CE) in the measured spectral region than it was reported in Ref. [51], although the positions and signs of the principal CEs (B, D, F) are identical. Moreover, the shapes and half-widths ($\Delta_{1/2}$) of the negative and positive low-energy CEs ($\Delta_{1/2}$ = 2.6 and 3.5, respectively) suggest that several electron transitions take place in this range. Our data for **III** are also in agreement with the detailed analysis of the AB spectra of $[Pd(allyl)Cl]_2$ (**VIII**) [54].

Three bands in the AB spectrum of **VIII** (29.5, 34.0, 40.5 kK) were attributed in Ref. [54] to d–d transitions from the MOs with the main contributions of d_{xz}-, d_{yz}-, and $d_{x^2-y^2}$-AOs, respectively, to the MO with the main contribution of d_{z^2}-AO (Fig. 13). We suppose that C, D, E bands in the CD spectrum of **III** (26.9, 29.9, 35.0 kK) correspond to the same dipole-allowed transitions (DAT) (Fig. 13). The choice of mononuclear fragment for analysis was based [46,55] on the absence of interaction between Pd atoms in dimers Pd_2X_6 and the similarity of AB spectra of PdX_4^{2-} and Pd_2X_6 in the region of d–d transitions.

Band B can be assigned to y-polarized magnetic-allowed transition (MAT) $d_{xz} - d_{z^2}$ coupled with DAT $d_{yz} - d_{z^2}$ (band D). The z-polarized MAT $d_{xy} - d_{z^2}$ probably also contributes to the D band. The negative CE resulted from $d_{x^2-y^2} - d_{z^2}$ DAT (coupled with $d_{xy} - d_{z^2}$) is almost compensated by positive CE in the region of charge transfer transition $p_{\pi Cl} - d_{z^2}$ (band F) and d–d transitions (band D).

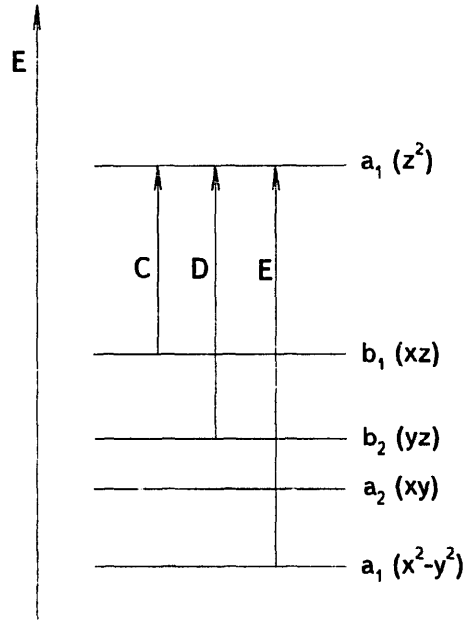

Fig. 13. Qualitative MO diagram and the suggested assignment of electron transitions in **III**.

A rather uniform bathochromic shift for C, D, E bands in the CD spectrum of **III** related to the positions of corresponding bands in AB spectrum of **VIII** can probably be explained by an increase of electron donor character in the case of β-pinenyl ligand. The analysis of CD spectrum of **III** confirms the applicability of the one-electron model of optical activity to metallochromophores [3].

4.2.2. *Optically active clusters I and II*

The AB spectra of **I** and **II**, similar to most other transition metal clusters [3,56], represent an increasing absorption without distinct maxima (Fig. 14). However, they are close to the AB spectra of **XI** and **XV** (Tables 7 and 8) pointing to a possible similarity of their structures. The better developed pattern in CD spectra of the chiral clusters in the measured spectral range

Table 8
AB and CD spectra of the $Fe_3MPdC(CO)_{12}(\eta^3\text{-}C_{10}H_{15})$ clusters in CH_2Cl_2 solution

$Fe_3CoPdC(CO)_{12}(\eta^3\text{-}C_{10}H_{15})$ (**I**)				$Fe_3RhPdC(CO)_{12}(\eta^3\text{-}C_{10}H_{15})$ (**II**)				Band
AB		CD		AB		CD		
ν, kK	ε	ν, kK	$\Delta\varepsilon$	ν, kK	ε	ν, kK	$\Delta\varepsilon$	
17.50 inflat	2210	15.50	+2.96	14.80sh	508	15.38sh	+0.08	A
		18.18sh	+4.50					
20.0sh	3316	18.59	+6.00	18.56sh	2539	19.60	+2.03	B
		22.12	−9.13	20.80 inflat	3945	24.10	−1.66	C
						27.78sh	+9.68	
31.0sh	21,056	28.57	+24.65	26.16sh	17,188	28.99	+10.39	D
36.5sh	29,215	> 32.26	−CE	33.0sh	25,000	> 33.3	−CE	
				38.0sh	38,672			

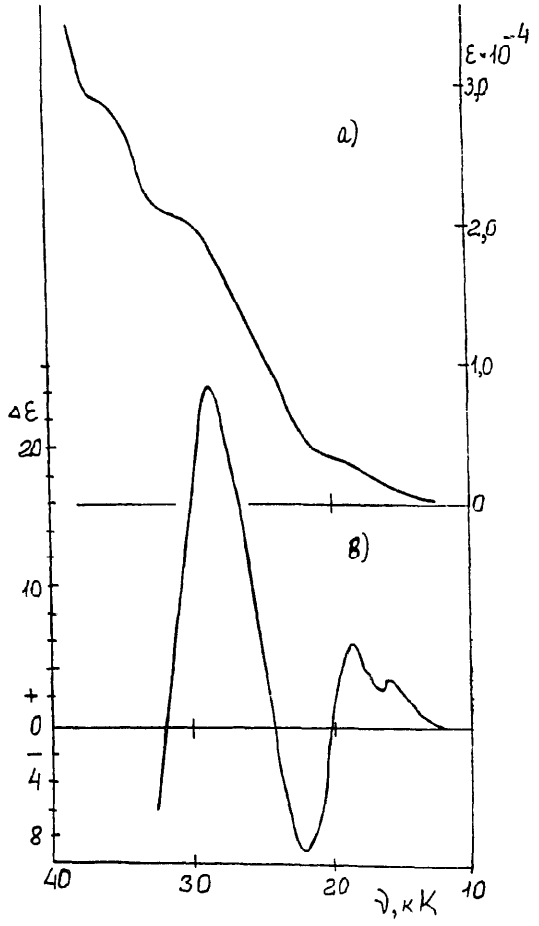

Fig. 14. AB (a) and CD (b) spectra of I.

displays four intense CEs (A–D) for I and three CEs (B–D) for II (Table 8). The intensity of CE at 28.57 kK is by far greater than corresponding CD features in the region of 25–35 kK observed for other studied chiral clusters [3,40,43,47,48].

Assuming the same absolute configuration for I–III (see above), we attribute the source of optical activity in I and II to [Pd(β-pinenyl)] fragment. Nevertheless, the positions and high intensities of CEs in the CD spectra of I and II compared to the spectrum of III evidently show that the observed CEs are induced in electron transitions of cluster metallochromophores due to a strong interaction of metal framework and the asymmetric [Pd(β-$C_{10}H_{15}$)] fragment. Such a strong manifestation of vicinal optical activity was observed for the first time and undoubtedly will be of much help in future studies of relationships between the stereochemistry and chiroptical properties of transition metal clusters.

Acknowledgements

This work was generously supported by the International Science Foundation (grants N91000, J88100 and MNC300) and by the Russian Foundation of Basic Researches (grants 93-03-5705, 96-03-33245 and 96-03-32684). Y.L.S. is indebted to Prof. Dmitri I. Kochubei for a research visit at the Siberian Synchrotron Radiation Source (Novosibirsk) and to Boris N. Novgorodov for a help in EXAFS data collection.

References

[1] S.P. Gubin, Koord. Khim. 20 (1994) 403, in Russian.
[2] S.P. Gubin, T.V. Galuzina, I.F. Golovaneva, A.P. Klyagina, Mendeleev Commun. 3 (1996) 87.
[3] A.P. Klyagina, I.F. Golovaneva, Metallorganich. Khim. 3 (1990) 503, in Russian.
[4] M. Tachikawa, R.L. Geerts, E.L. Muetterties, J. Organomet. Chem. 213 (1981) 11.
[5] Ya.V. Zubavichus, T.V. Galuzina, Ol.A. Beliakova, S.P. Gubin, Yu.L. Slovokhotov, Yu.T. Struchkov, Mendeleev commun., (1995) 91.
[6] A.P. Klyagina, T.V. Misailova, I.F. Golovaneva, S.P. Gubin, Izv. Akad. Nauk. Ser. Khim. 6 (1996) 1559, in Russian.
[7] S.P. Gubin, L.A. Polyakova, T.V. Galuzina, Koord. Khim. 23 (1997) 102, in Russian.
[8] J.A. Cleverty, G. Wilkirson, in: H.F. Holtzelaw (Ed.), Inorg. Synthesis, 8 (1966) 211.
[9] G. Brauer (Ed.), Rukovodstvo po neorganicheskomu sinte zu, 6 (1986) p. 2117 (in Russian).
[10] V.E. Lopatin, S.P. Gubin, N.M. Mikova, Tsybenov M.Ts, Yu.L. Slovokhotov, Yu.T. Struchkov, J. Organomet. Chem. 292 (1985) 275.
[11] G. Brauer (Ed.), Rukovodstvo po neorganicheskomu sinte zu. 5 (1986) p. 1001 (in Russian).
[12] B.M. Trost, P.E. Strege, L. Weber, T.J. Fullerton, T.J. Dietsche, J. Am. Chem. Soc. 100 (1978) 3407.
[13] K. Dunne, F.J. McQuillin, J. Chem. Soc. C. 16 (1970) 2200.
[14] J.W. Kolis, E.M. Holt, D.F. Shriver, J. Am. Chem. Soc. 105 (1983) 7307.
[15] M. Tachikawa, E.L. Muetterties, Prog. Inorg. Chem. 24 (1981) 203.
[16] J.A. Hriljac, P.N. Swepston, D.F. Shriver, Organometallics 4 (1985) 158.
[17] A.V. Iljasov, Yu.M. Kargin, Izv. Akad. Nauk. Ser. Khim. 5 (1971) 927, in Russian.
[18] G.M. Sheldrick, SHELXL-93. Program for the refinement of crystal structures. University of Goettingen, Germany, 1993.
[19] F.H. Allen, S.A. Bellard, M.D. Brice, B.A. Cartwright, A. Doubleday, H. Higgs, T. Hummelink-Peters, O. Kennard, W.D.S. Mothherrwell, J.R. Rodgeeerrs, D.G. Watson, Acta Crystallogr. B 35 (1979) 2331.
[20] A.S. Gunale, M.P. Jensen, Ch.L. Stern, D.F. Shriver, J. Am. Chem. Soc. 113 (1991) 1458.
[21] J.W. Kolis, E.M. Holt, J.A. Hriljac, D.F. Shriver, Organometallics 3 (1984) 496.
[22] S.P. Gubin, G.V. Burmakina, T.V. Galuzina, Koord. Khim. 21 (1995) 731, in Russian.
[23] S.P. Gubin, Pure Appl. Chem. 58 (1986) 567.
[24] S.P. Gubin, T.V. Galuzina, P.A. Koz'min, M.D. Surajskaya, T.B. Larina, Koord. Khim. 20 (1994) 665, in Russian.
[25] M.Ts. Tsybenov, S.P. Gubin, V.E. Lopatin, N.C. Erdineev, Zh. Vses. Khim. Obshch. imeni Mendeleeva 32 (1987) 104, in Russian.
[26] R.D. Macfarlane, Mass Spectrom. Rev. 4 (1985) 421.

[27] V.E. Lopatin, V.E. Ershova, M.Ts. Tsybenov, S.P. Gubin, Akad. Nauk. Ser. Khim. 11 (1984) 2648, in Russian.
[28] J.A. Hriljac, E.M. Holt, D.F. Shriver, Inorg. Chem. 26 (1987) 2943.
[29] S.P. Gubin, Koord. Khim. 21 (1995) 659, in Russian.
[30] C. Thone, H. Vahrenkamp, J. Organomet. Chem. 485 (1995) 185.
[31] B.F.G. Jonson, D.A. Kaner, J. Lewis, P.R. Raithby, M.J. Rosales, J. Organomet. Chem. 231 (1982) 59.
[32] P.S. Pregosin, H. Ruegger, R. Salzmann, A. Albinati, F. Lianza, R.W. Kunz, Organometallics 13 (1994) 83.
[33] C.J. Amman, P.S. Pregosin, H. Ruegger, R. Salzmann, A. Albinati, F. Lianza, R.W. Kunz, J. Organomet. Chem. 423 (1992) 415.
[34] K. Wade, Chem. Commun., (1971) 792.
[35] Yu.L. Slovokhotov, Yu.T. Struchkov, J. Organomet. Chem. 333 (1987) 217.
[36] R.S. Cahn, C.K. Ingold, V. Prelog, Angew. Chem., Int. Ed. 5 (1966) 385.
[37] K. Schlogl, M. Fried, H. Falk, Monatsh. Chem. 95 (1964) 576.
[38] D. Marguarding, H. Klusacek, G. Ganel, P. Hoffman, I. Ugi, J. Amer. Chem. Soc. 92 (1970) 5389.
[39] H. Vahrenkamp, J. Organomet. Chem. 370 (1989) 65.
[40] F. Richter, H. Vahrenkamp, Angew. Chem. Int. Ed. 19 (1980) 65.
[41] M. Muller, H. Vahrenkamp, Chem. Ber. 116 (1983) 2748.
[42] R. Blumhofer, H. Vahrenkamp, Chem. Ber. 119 (1986) 683.
[43] A.J. Arce, A.Y. Deeming, J. Chem. Soc. Chem. Commun., (1980) 1102.
[44] V.A. Maksakov, V.A. Ershova, V.P. Kirin, I.F. Golovaneva, A.Ya. Mikhailova, A.P. Klyagina, Dokl. Akad. Nauk SSSR 299 (1988) 1142.
[45] V.A. Maksakov, V.P. Kirin, A.V. Golovin, Izv. Akad. Nauk. Ser. Khim. (1995) 2021.
[46] J. Collin, C. Jossart, G. Balavoine, Organometallics 5 (1986) 203.
[47] C. Mahe, M. Patin, J.-Y. Le Maronille, A. Benoit, Organometallics 2 (1983) 1051.
[48] H. Brunner, M. Muschiol, J. Organomet. Chem. 248 (1983) 233.
[49] G. Consiglio, R.M. Waymouth, Chem. Rev. 1 (1989) 257.
[50] A. Pfaltz, in: E. Ottow, K. Schollkopf, B.-G. Sculz (Eds.), Stereoselective Syntesis, Springer-Verlag, Berlin, 1994, p. 15.
[51] A.I. Scott, A.D. Wrixon, Tetrahedron 27 (1971) 2339.
[52] J.A. Schellman, J. Chem. Phys. 44 (1966) 55.
[53] S.F. Mason, Molecular Optical Activity and Chiral Discrimination, Cambridge Univ. Press, 1982.
[54] F.R. Hartley, J. Organomet. Chem. 21 (1970) 227.
[55] W.R. Mason, H.B. Gray, J. Amer. Chem. Soc. 90 (1968) 5721.
[56] I.F. Golovaneva, T.V. Misailova, A.P. Klyagina, S.P. Gubin, Koord. Khim. 21 (1995) 668, in Russian.